Wefer, G., Berger, W.H., and Richter, C. (Eds.)
Proceedings of the Ocean Drilling Program, Scientific Results Volume 175

15. Data Report: Petrographic, Cathodoluminescent, and Compositional Characteristics of Organogenic Dolomites from the Southwest African Margin[1]

Peir K. Pufahl[2] and Gerold Wefer[3]

INTRODUCTION

The main objective of Leg 175 was to reconstruct the Late Neogene paleoceanographic history of the Benguela Current and associated upwelling regimes along the southwest African margin between 5° and 32°S. This area is one of the great upwelling regions of the world and plays an important role in the global ocean–carbon cycle. It is characterized by organic-rich sediments that contain a high-resolution record of productivity history that is closely linked to changes in regional dynamics of circulation, mixing, and upwelling (Wefer et al., 1998). The Benguela Current region also provides an excellent setting to investigate the early diagenetic processes governing the formation of authigenic dolomite. Although unexpected, the discovery of widespread and pervasive dolomite horizons along the southwest African margin was one of the principal findings of Leg 175.

Dolomite precipitation within upwelling regimes is stimulated by the effects of high productivity and occurs early within the uppermost tens to hundreds of meters of sediment (Garrison et al., 1984; Hay, Sibuet, et al., 1984; Kastner et al., 1990; Kelts and McKenzie, 1982; Kulm et al., 1984; Lyle, Koizumi, Richter, et al., 1997; Middelburg et al., 1990; Pisciotto and Mahoney, 1981; Suess et al., 1988). Productivity must be sufficiently high to generate a favorable environment; the microbial respiration of sedimentary organic matter increases alkalinity and pH of

[1]Pufahl, P.K., and Wefer, G., 2001. Data report: Petrographic, cathodoluminescent, and compositional characteristics of organogenic dolomites from the southwest African margin. *In* Wefer, G., Berger, W.H., and Richter, C. (Eds.), *Proc. ODP, Sci. Results,* 175, 1–17 [Online]. Available from World Wide Web: <http://www-odp.tamu.edu/publications/175_SR/VOLUME/CHAPTERS/SR175_15.PDF>. [Cited YYYY-MM-DD]
[2]The Department of Earth and Ocean Sciences, The University of British Columbia, 6339 Stores Road, Vancouver BC V6T 1Z4, Canada. **ppufahl@eos.ubc.ca**
[3]Faculty of Earth Sciences (FB 5), University of Bremen, Postfach 33 04 40, 28334 Bremen, Federal Republic of Germany.

Initial receipt: 16 October 2000
Acceptance: 5 February 2001
Web publication: 5 June 2001
Ms 175SR-234

pore waters and simultaneously alters Mg-Ca solution and crystal surface chemistries to promote dolomite precipitation (Baker and Burns, 1985; Baker and Kastner, 1981; Compton and Siever, 1986; Compton, 1988; Compton et al., 1994; Hardie, 1987; Mazzullo, 2000; Slaughter and Hill, 1990; Vasconcelos and McKenzie, 1997). These organogenic dolomites are distinguished from other types of authigenic carbonates by having a significant portion of their carbon derived from microbially degraded organic carbon (Froelich et al., 1979) and are thus characterized by $\delta^{13}C$ values that deviate strongly from those of normal marine carbonates (Friedman and Murata, 1979; Irwin et al., 1977; Murata et al., 1972; Pisciotto and Mahoney, 1981).

Here, we report the occurrence of organogenic dolomite horizons within organic-rich Neogene and Quaternary hemipelagic sediments from the southwest African margin. The purpose of this paper is to document the mineralogical, compositional, textural, and cathodoluminescent (CL) properties of dolomite horizons. It is not within the scope of this report to discuss horizon formation in detail. Aspects of horizon development based on the interpretation of these properties will be the focus of a subsequent paper.

METHODS

The petrography of dolomite samples was studied using transmitted light microscopy complemented with back-scattered electron (BSE) imaging and microprobe analyses of selected polished thin sections. CL investigation of specimens was performed using a Nuclide ELM-3R luminiscope coupled to a SPEX 1681 spectrophotometer operating at 2.6 Pa with an excitation voltage of 10 kV. CL photomicrographs were taken at very long exposure times of 10–20 min because sample luminosities were extremely low. BSE photomicrographs and energy-dispersive X-ray spectra of dolomite phases were acquired with a Philips XL-30 scanning electron microscope equipped with a Princeton Gamm-Tech thin-window detector. Fe and Mn contents of dolomite samples were collected using a fully automated CAMECA SX-50 microprobe operating in the wavelength-dispersive mode, with the following operating conditions: excitation voltage = 15 kV, beam current = 10 nA, peak count time = 20 s. Data reduction was done with the "PAP" $\phi(\rho Z)$ method (Pouchou and Pichoir, 1985). Chemical formulas were normalized on six anions assuming two carbon atoms per formula unit. Step-scan X-ray powder diffraction data were collected over the range 3°–60°2θ with CuK_α radiation using a Siemens D5000 Bragg-Brentano diffractometer equipped with a diffracted-beam graphite monochronometer crystal, 2-mm (1°) divergence and anti-scatter slits, 0.6-mm receiving slit, and incident-beam Soller slit. A profile-fitting program provided by Siemens using the ICDD PDF-2 database was utilized to identify X-ray peaks. Carbon and oxygen isotope analyses of dolomite samples were performed at Bremen University. Six to thirteen subsamples were taken from each specimen. Values in the text are averages calculated from individual data sets. Carbon and oxygen isotopic results are reported in per mil relative to the Peedee belemnite (PDB) standard.

DOLOMITE OCCURRENCE

Dolomite horizons occur as discrete centimeter-thick layers within Cenozoic organic-rich hemipelagites from the Angola Basin and Walvis Ridge and Basin (Fig. F1) (Pufahl et al., 1998; Wefer et al., 1998). In the Angola Basin, authigenic layers were intersected at Sites 1078 and 1080 within moderately bioturbated Holocene to Pleistocene calcareous clays containing high proportions of silt and organic carbon of mixed marine-terrestrial origin (total organic carbon [TOC] values range from 1.11 to 5.35 wt%) (Table T1). The clastic fraction is dominated by silt-sized grains of smectite, kaolinite, and/or illite, muscovite, quartz, albite, and microcline. Framboidal and subhedral pyrite are common accessory phases. Sedimentation within the Angola Basin records moderate levels of productivity within a coastal environment free of strong fluvial and upwelling influences. Deposition is dominated by the offshore transport and hemipelagic rain out of silts and clays derived from vigorous coastal erosion (Berger et al., 1998). Sedimentation rates are consequently extremely high with maximum values of 60 cm/k.y.

Site 1078 is located in 427 m of water between the high-productivity regions of the Congo River to the north and the Namibia coast to the south. Several dolomite layers were recovered from this site at depths of 83, 112, and 131 meters below seafloor (mbsf). Three intervals of laminated sediments consisting of intercalated diatom mats and thinly bedded Bouma division DE turbidites were also intersected at Site 1078. The authigenic layer at 131 mbsf occurs within the upper portion of a laminated interval. Dolomite horizons at 83 and 112 mbsf occur in nannofossil-rich clay. Site 1080 is located in 2766 m of water north of the Walvis Ridge. At Site 1080, much of the late Quaternary record is missing and dolomite horizons were intersected at shallower depths of 38 and 51 mbsf in Pleistocene nannofossil- and foraminifer-rich clay. Sediments from Site 1080 represent a disturbed and incomplete hemipelagic succession recording successive episodes of winnowing associated with stratigraphic condensation. The presence of intervals of laminated sediment and benthic foraminifers tolerant of low-oxygen conditions indicates that bottom waters in the Angola Basin have had persistent low-oxygen concentrations.

Sites 1081 and 1082 are located in 760 and 1279 m of water, respectively, within the Walvis Basin (Table T1). Sediments at each site span the late Miocene to Holocene and consist of organic-rich (TOC values range from 0.03 to 16.08 wt%) pyrite-bearing calcareous clays with varying abundances of foraminifers, diatoms, and nannofossils. As in the Angola Basin, the clastic fraction consists of silt-sized grains of smectite, kaolinite, and/or illite, muscovite, quartz, albite, and microcline. Although the sites are seaward of the upwelling center, they contain a strong upwelling signal that has been transported outward from its coastal zone by eddies and filaments of the Benguela Current. Sediment accumulation rates at the Walvis sites are typically between 5 and 10 cm/k.y. but can be as high as 20 cm/k.y.

Fifty-three dolomite horizons were found within sediments from Sites 1081 and 1082. Horizons were identified mainly on the basis of downhole logging but were verified through samples in cores. Holes were logged four times. The first tool string (siesmostratigraphy) included the spectral gamma-ray (NGT), sonic, electrical induction, and temperature (TLT) sondes. This combination is useful for describing lithology, sedimentary fabric, and degree of lithification. The second tool

F1. Location map of ODP Leg 175 sites, p. 11.

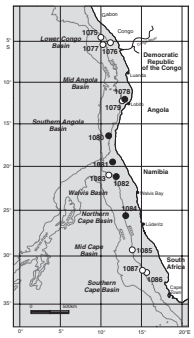

T1. Stratigraphic, compositional, luminescent, and isotopic data for dolomite samples, p. 16.

string (lithoporosity) included the NGT, neutron porosity, gamma density, and TLT sondes. The third tool string (Formation MicroScanner [FMS], two passes) included the NGT, inclinometer, and FMS sondes. The FMS tool string produces high-resolution electrical resistivity images of the borehole wall, which can be used to study the bedding structures and diagenetic features. The fourth tool string (geological high-sensitivity magnetic tool [GHMT]) included the NGT, magnetic susceptibility, and vertical component magnetometer. This string provides a magnetic stratigraphy of the sediments. Distinct spikes in resistivity, density, and sound velocity downhole are interpreted as discrete dolomite horizons. Because of their high resistivity, these layers are readily identifiable by FMS (Wefer et al., 1998). Of the 53 dolomite horizons identified, only 16 were recovered during drilling.

Site 1084 is located within the Northern Cape Basin, north of Lüderitz, in 1992 m of water where filaments of cold nutrient-rich water from the coastal upwelling area mix with lower productivity oceanic water, producing a zone of intermediate productivity. Sediments range in age from early Pliocene to Pleistocene and consist of bioturbated clays containing varying abundances of diatoms, nannofossils, foraminifers, and radiolarians (Table **T1**). Sediments here contain the highest organic carbon contents of any site studied during Leg 175 (TOC values are as high as 18.01 wt%). Diagenetic activity, as reflected in the ubiquitous presence of carbon dioxide and methane and in the rapid reduction of sulfate within pore waters, is intense; alkalinity concentrations reached a maximum value of 172 mM, which is the second highest ever measured in sediments recovered by the Deep Sea Drilling Project (DSDP) or the Ocean Drilling Program (ODP) (Murray et al., 1998). Sedimentation rates vary between 10 and 27 cm/k.y.

Dolomite horizons from Walvis Ridge and Basin and Cape Basin sites are 10 to 60 cm thick and are restricted to intervals of sediment below 100 mbsf. Two types of dolomite horizons were recovered: lithified and semilithified (Fig. **F2A, F2B**). Lithified layers commonly possess a hard center that becomes increasingly less cemented above and below. Semilithified horizons are friable and disaggregate easily and were only intersected at Site 1081; they have high intercrystalline porosities that range from 20% to 25%. Porosities of lithified layers are much lower and are typically between 5% and 7%. A continuum exists between these two end-members that reflects the relative degree of authigenesis. There appears to be no obvious relationship between host sediment composition and horizon type. The lateral extent of horizons is unknown, but by analogy with similar authigenic carbonate layers that punctuate compositionally similar Cenozoic strata in the circum-Pacific region, we assume that layers pinch and swell over a distance of a few hundred meters (Garrison et al., 1984, and references therein; Pisciotto and Mahoney, 1981).

No dolomite was found at Site 1083, located only 25 km to the northwest of Site 1082 but at greater water depth (2200 m). Carbonate contents at Site 1083 are relatively high (carbonate carbon values range from 19.8 to 82.2 wt%), and organic carbon values are lower than the other sites (TOC values range from 1.02 to 5.52 wt%).

F2. Photomicrographs of dolomite horizons, p. 12.

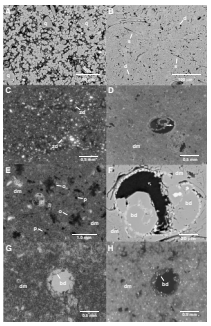

CATHODOLUMINESCENT AND TRANSMITTED LIGHT PETROGRAPHY

CL microscopy is a complementary technique to standard petrographic methods that has revolutionized the way in which carbonates are interpreted. Three areas of application are common: (1) making fabrics visible that are not visible by standard petrographic microscopy, such as recrystallization nuclei; (2) "cement stratigraphy," that is, the correlation in carbonate rocks by interpreting equally luminescent zones as diagenetically coeval; and (3) geochemical interpretation of redox-sensitive trace elements incorporated into the crystal structure at the time of precipiation (Machel, 1985). Mn^{2+} appears to be the most important element causing luminescence in natural carbonates, because it is relatively abundant and generates intense emission (Machel et al., 1991). Fe^{2+} is the single most important element in quenching luminescence (Machel and Burton, 1991; Machel et al., 1991). For a detailed overview of CL and its petrographic applications, the reader is referred to Barker and Kopp (1991) and references therein. Three types of dolomite were identified within samples based on their mode of occurrence in thin section and CL properties. These are (1) dolomicrite; (2) blocky, void-filling dolomite; and (3) fine silt-sized, zoned, rhombohedral dolomite. These phases record progressive degrees of induration associated with horizon development and burial.

Dolomicrite

Dolomicrite is the dominant horizon-forming phase and consists of sucrosic mosaics of interlocking subhedral, equigranular dolomite rhombs that form olive-green authigenic horizons with a "fitted fabric." Rhombs are typically 10 µm in diameter, have grown within pore spaces as an intergranular cement, and have planar, irregular, compromise crystal boundaries. Hypidiotopic crystalline aggregates commonly envelop diatom and foraminifer tests, fish bones, subhedral pyrite grains, and luminescent, pyrite-rich organic blebs (Fig. **F2E**). Pyrite grains are a common accessory phase and are commonly enveloped by a 1- to 2-µm-thick rim of luminescent dolomite (Fig. **F2C**). Foraminifer tests are typically well preserved. Recrystallized skeletons are present only within lithified horizons where the outer margins of shell walls are altered, forming a thin, luminescent intraparticle lining (Fig. **F2D**). Fish bones enveloped by dolomite crystals show evidence of dissolution along their margins.

Dolomicrites can be divided, based on their CL properties, into luminescent, weakly luminescent, and nonluminescent varieties. CL spectra and microprobe analysis indicate that cathodoluminescence is Mn-activated and Fe-quenched (Fig. **F3**). Luminescent layers are characterized by an orange-brown color and a blotchy, mottled texture when viewed with CL (Fig. **F2H**). Weakly luminescent dolomicrites are a dull brown-orange color and exhibit a shift in their emission spectra towards longer wavelengths caused by crystallographic distortions in the coordination of Mn^{2+} induced by high quencher concentrations of Fe^{2+} (Machel, 1985; Machel et al., 1991).

F3. CL spectrum showing Mn-activated luminescence, p. 14.

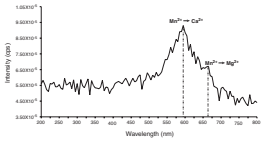

Blocky Dolomite

Blocky dolomite occurs only within lithified dolomite horizons and becomes increasingly more abundant in samples from deeper stratigraphic levels. It consists of blocky nonluminescent dolomite crystals with planar boundaries that infill foraminifer and diatom tests (Fig. F2F, F2G, F2H). Crystals are larger than those forming dolomicrite, ranging in size from 15 to 20 µm. In many instances, the intraparticle pores within tests have been entirely occluded by blocky dolomite. Blocky dolomite was not observed in semilithified horizons recovered from Site 1081.

Zoned Dolomite

Zoned dolomite is found only in the Angola Basin at Site 1078 within the interval of laminated sediments at 131 mbsf. It occurs as disseminated, euhedral rhombohedra within the bases of authigenically cemented Bouma DE turbidites. Rhombs consist of an abraded, detrital core and an outer authigenic rim. Crystal size is more variable than in the dolomicrites and void-filling dolomites, typically ranging from 5 to 12 µm.

CL study of zoned dolomites confirms what transmitted light petrography suggests, that euhedral dolomite crystals within turbidites consist of a central core of detrital dolomite and an outer rim (Fig. F2C). Rims are distinguished from cores by differences in luminescent character and zoning discontinuities across core margins. Cores typically consist of concentrically or oscillatory zoned silt-sized dolomite grains. Rims consist of a single luminescent zone of dolomite 1 to 2 µm thick. These characteristics are easily viewed by the naked eye under CL but are difficult to discern in photomicrographs of zoned dolomites because the small crystal size and long exposure times required prevents adequate resolution of these features. The common presence of luminescent dolomite rims around subhedral pyrite grains and detrital dolomite cores suggests that dolomite authigenesis commenced in the zone of sulfate reduction soon after the formation of pyrite. This interpretation is supported by studies that indicate that iron concentrations within this zone are maintained at low levels because of its incorporation into diagenetic pyrite (Berner, 1984, 1985; Burns and Baker, 1987; Hesse, 1990; Lyons and Berner, 1992; Murata et al., 1972). Pyrite forms through a series of metastable reactions when Fe^{2+}, derived from redox-controlled cation exchange reactions of clay minerals and dissolution of Fe oxides, combines with sulfide produced from the microbial reduction of porewater sulfate. These early diagenetic reactions preclude the incorporation of Fe^{2+} in dolomite precipitating within the zone of sulfate reduction, producing the luminescent dolomite rims observed in thin section.

CRYSTAL CHEMISTRY

Dolomites are calcium rich and have the general chemical formula $Ca_{1.04–1.13}(Mg_{0.83–0.94}Fe_{0.01–0.04})_{\varepsilon 0.84–0.98}(CO_3)_2$. Although CL spectra indicate that CL is Mn-activated, Mn is below the detection limits of the microprobe and is therefore not included in the general chemical formula. Weakly luminescent dolomicrites contain as much as 3.2× the amount of Fe as luminescent varieties (Table T2). Blocky dolomite can

T2. Electron microprobe analyses of iron concentrations in dolomite, p. 17.

contain ~1.4× the amount of iron as weakly luminescent dolomicrites and 4.4× the amount of iron as luminescent dolomicrites (Table T2). The high iron contents of these dolomites reflects their precipitation in a reducing environment (McHargue and Price, 1982).

X-ray diffractograms of semilithified and lithified authigenic layers are shown in Figure F4 with hexagonal reference indices (Lippmann, 1973). Diffractograms show sharply defined peaks, including superstructure reflections. The presence of the (101), (015), (021), and (009) superstructure reflections (Reeder, 1990) indicates that both lithified and semilithified horizons are formed of well-ordered dolomite.

Dolomite samples from the Angola Basin, Walvis Ridge and Basin, and the Northern Cape Basin show extreme enrichment in $\delta^{13}C$ values with values as great as 16.85‰ and an average 9.39‰ (PDB) for 18 samples (Table T1). Following the models of Claypool and Kaplan (1974) and Irwin et al. (1977), we interpret the "heavy" $\delta^{13}C$ values of dolomite horizons (Table T1) as evidence that after the initial precipitation of dolomite within the zone of sulfate reduction, authigenesis continued with progressive burial into the zone of methanogenesis, where the bulk of dolomite was formed. The $\delta^{18}O$ signature varies between 2.87‰ and 6.50‰ (PDB).

F4. X-ray diffractograms of semilithified and lithified horizons, p. 15.

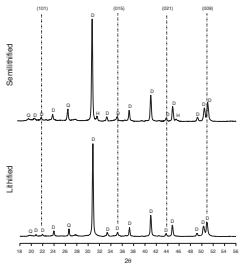

ACKNOWLEDGMENTS

We thank the technicians, scientists, and crew of Leg 175 for their help throughout the cruise. We gratefully acknowledge the Ocean Drilling Program for providing the samples used in this study. R.E. Garrison, L.A. Groat, and L.D. Anderson provided critical reviews of the manuscript. The German Research Foundation (SPP DSDP/ODP) provided funding for the stable isotopic analyses of dolomite samples. NSERC provided funding through an operating grant to K.A. Grimm and a postgraduate scholarship to P.P. This research was also supported by a University Graduate Fellowship from The University of British Columbia and a Killam Predoctoral Fellowship to P.P.

REFERENCES

Baker, P.A., and Burns, S.J., 1985. The occurrence and formation of dolomite in organic-rich continental margin sediments. *AAPG Bull.,* 69:1917–1930.

Baker, P.A., and Kastner, M., 1981. Constraints on the formation of sedimentary dolomite. *Science,* 213:215–216.

Barker, C.E., and Kopp, O.C., 1991. *Luminescence Microscopy and Spectroscopy: Qualitative and Quantitative Applications*. SEPM Short Course, 25.

Berger, W.H., Wefer, G., Richter, C., Lange, C.B., Giraudeau, J., Hermelin, O., and Shipboard Scientific Party, 1998. The Angola-Benguela upwelling system: paleoceanographic synthesis of shipboard results from Leg 175. *In* Wefer, G., Berger, W.H., and Richter, C., et al., *Proc. ODP, Init. Repts.,* 175: College Station, TX (Ocean Drilling Program), 505–531.

Berner, R.A., 1984. Sedimentary pyrite formation: an update. *Geochim. Cosmochim. Acta,* 48:605–615.

————, 1985. Sulfate reduction, organic matter decomposition, and pyrite formation. *Philos. Trans. R. Soc. London,* 315:25–38.

Burns, S.J., and Baker, P.A., 1987. A geochemical study of dolomite in the Monterey formation, California. *J. Sediment. Petrol.,* 57:128–139.

Claypool, G.E., and Kaplan, I.R., 1974. The origin and distribution of methane in marine sediments. *In* Kaplan, I.R. (Ed.), *Natural Gases in Marine Sediments:* New York (Plenum), 99–139.

Compton, J.S., 1988. Degree of supersaturation and precipitation of organogenic dolomite. *Geology,* 16:318–321.

Compton, J.S., Donald, H.L., Mallinson, D.J., and Hodell, D.A., 1994. Origin of dolomite in the phosphatic Miocene Hawthorn Group of Florida. *J. Sediment. Res.,* 64:638–649.

Compton, J.S., and Siever, R., 1986. Diffusion and mass balance of Mg during early dolomite formation, Monterey Formation. *Geochim. Cosmochim. Acta,* 50:125–135.

Friedman, I., and Murata, K.J., 1979. Origin of dolomite in Miocene Monterey shale and related formations of the Temblor Range, California. *Geochim. Cosmochim. Acta,* 43:1357–1365.

Froelich, P.N., Klinkhammer, G.P., Bender, M.L., Luedtke, N.A., Heath, G.R., Cullen, D., Dauphin, P., Hammond, D., Hartman, B., and Maynard, V., 1979. Early oxidation of organic matter in pelagic sediments of the eastern equatorial Atlantic: suboxic diagenesis. *Geochim. Cosmochim. Acta,* 43:1075–1090.

Garrison, R.E., Kastner, M., and Zenger, D.H., 1984. *Dolomites of the Monterey Formation and Other Organic-Rich Units*. Soc. Econ. Paleontol. Mineral., Pacific Sect., 41.

Hardie, L.A., 1987. Dolomitization: a critical view of some current views. *J. Sediment. Petrol.,* 57:166–183.

Hay, W.W., Sibuet, J.-C., et al., 1984. *Init. Repts. DSDP,* 75: Washington (U.S. Govt. Printing Office).

Hesse, R., 1990. Early diagenetic pore water/sediment interaction: modern offshore basins. *In* McIlreath, I.A., and Morrow, D.W. (Eds.), *Diagenesis:* Ottawa, ON (Geoscience Canada), 277–316.

Irwin, H., Curtis, C., and Coleman, M., 1977. Isotopic evidence for source of diagenetic carbonates formed during burial of organic-rich sediments. *Nature,* 269:209–213.

Kastner, M., Elderfield, H., Martin, J.B., Suess, E., Kvenvolden, K.A., and Garrison, R.E., 1990. Diagenesis and interstitial-water chemistry at the Peruvian continental margin—major constituents and strontium isotopes. *In* Suess, E., von Huene, R., et al., *Proc. ODP, Sci. Results,* 112: College Station, TX (Ocean Drilling Program), 413–440.

Kelts, K., and McKenzie, J.A., 1982. Diagenetic dolomite formation in Quaternary anoxic diatomaceous muds of Deep Sea Drilling Project Leg 64, Gulf of California.

In Curray, J.R., Moore, D.G., et al., *Init. Repts. DSDP,* 64 (Pt. 2): Washington (U.S. Govt. Printing Office), 553–569.

Kulm, L.D., Suess, E., and Thornburg, T.M., 1984. Dolomites in the organic-rich muds of the Peru forearc basins: analogue to the Monterey Formation. *In* Garrison, R.E., Kastner, M., and Zenger, D.H. (Eds.), *Dolomites in the Monterey Formation and Other Organic-rich Units*. Spec. Publ.—Soc. Econ. Paleontol. Mineral., 41:29–48.

Lippmann, F., 1973. *Sedimentary Carbonate Minerals:* New York (Springer Verlag).

Lyle, M., Koizumi, I., Richter, C., et al., 1997. *Proc. ODP, Init. Repts.,* 167: College Station, TX (Ocean Drilling Program).

Lyons, T.W., and Berner, R.A., 1992. Carbon-sulfur-iron systematics of the uppermost deep-water sediments of the Black Sea. *Chem. Geol.,* 99:1–27.

Machel, H.G., 1985. Cathodoluminescence in calcite and dolomite and its chemical interpretation. *Geosci. Can.,* 12:139–147.

Machel, H.G., and Burton, E.A., 1991. Factors governing the cathodoluminescence in calcite and dolomite, and their implications for studies of carbonate diagenesis. *In* Barker, C.E., and Kopp, O.C. (Eds.), *Luminescence Microscopy and Spectroscopy: Qualitative and Quantitative Applications*. SEPM Short Course, 25:37–57.

Machel, H.G., Mason, R.A., Mariano, A.N., and Mucci, A., 1991. Causes and measurements of luminescence in calcite and dolomite. *In* Barker, C.E., and Kopp, O.C. (Eds.), *Luminescence Microscopy and Spectroscopy: Qualitative and Quantitative Applications*. SEPM Short Course, 25:9–25.

Mazzullo, S.J., 2000. Organogenic dolomitization in peritidal to deep-sea sediments. *J. Sediment. Res.,* 70:10–23.

McHargue, T.R., and Price, R.C., 1982. Dolomite clay in argillaceous or shale-associated marine carbonates. *J. Sediment. Petrol.,* 52:873–886.

Meyers, P.A., and Shipboard Scientific Party, 1998. Microbial gases in sediments from the southwest African margin. *In* Wefer, G., Berger, W.H., and Richter, C., et al., *Proc. ODP, Init Repts.,* 175: College Station, TX (Ocean Drilling Program), 555–560.

Middelburg, J.J., de Lange, G.J., and Kreulen, R., 1990. Dolomite formation in anoxic sediments of Kau Bay, Indonesia. *Geology,* 18:399–402.

Murata, K.J., Friedman, I., and Cremer, M., 1972. Geochemistry of diagenetic dolomites in Marine formations of California and Oregon. *U.S. Geol. Surv. Prof. Pap.,* 724-C.

Murray, R.W., Wigley, R., and Shipboard Scientific Party, 1998. Interstitial water chemistry of deeply buried sediments from the southwest African margin: a preliminary synthesis of results from Leg 175. *In* Wefer, G., Berger, W.H., and Richter, C., et al., *Proc. ODP, Init Repts.,* 175: College Station, TX (Ocean Drilling Program), 547–553.

Pisciotto, K.A., and Mahoney, J.J., 1981. Isotopic survey of diagenetic carbonates, Deep Sea Drilling Project, Leg 63. *In* Yeats, R.S., Haq., B.U., et al., *Init. Repts. DSDP,* 63: Washington (U.S. Govt. Printing Office), 595–609.

Pouchou, J.L., and Pichoir, F., 1985. PAP $\phi(\rho Z)$ procedure for improved quantitative microanalysis. *Microbeam Analysis 1985,* 104–106.

Pufahl, P.K., Maslin, M.A., Anderson, L., Brüchert, V., Jansen, F., Lin, H., Perez, M., Vidal, L., and Shipboard Scientific Party, 1998. Lithostratigraphic summary for Leg 175: Angola–Benguela upwelling system. *In* Wefer, G., Berger, W.H., and Richter, C., et al., *Proc. ODP, Init Repts.,* 175: College Station, TX (Ocean Drilling Program), 533–542.

Reeder, R.J., 1990. *Carbonates: Mineralogy and Chemistry.* Mineral. Soc. Am.

Slaughter, M., and Hill, R.J., 1990. The influence of organic matter in organogenic dolomitization. *J. Sediment. Petrol.,* 61:296–303.

Suess, E., von Huene, R., and the Leg 112 Shipboard Scientists, 1988. Ocean Drilling Program Leg 112, Peru continental margin: Part 2, Sedimentary history and diagenesis in a coastal upwelling environment. *Geology,* 16:939–943.

Vasconcelos, C., and McKenzie, J.A., 1997. Microbial mediation of modern dolomite precipitation and diagenesis under anoxic conditions (Lagoa Vermelha, Rio de Janeiro, Brazil). *J. Sediment. Res.,* 67:378–390.

Wefer, G., Berger, W.H., Richter, C., and Shipboard Scientific Party, 1998. Facies patterns and authigenic minerals of upwelling deposits off southwest Africa. *In* Wefer, G., Berger, W.H., and Richter, C., et al., *Proc. ODP, Init Repts.,* 175: College Station, TX (Ocean Drilling Program), 487–504.

Figure F1. Location map of ODP Leg 175 sites. Solid circles are those with authigenic dolomite horizons.

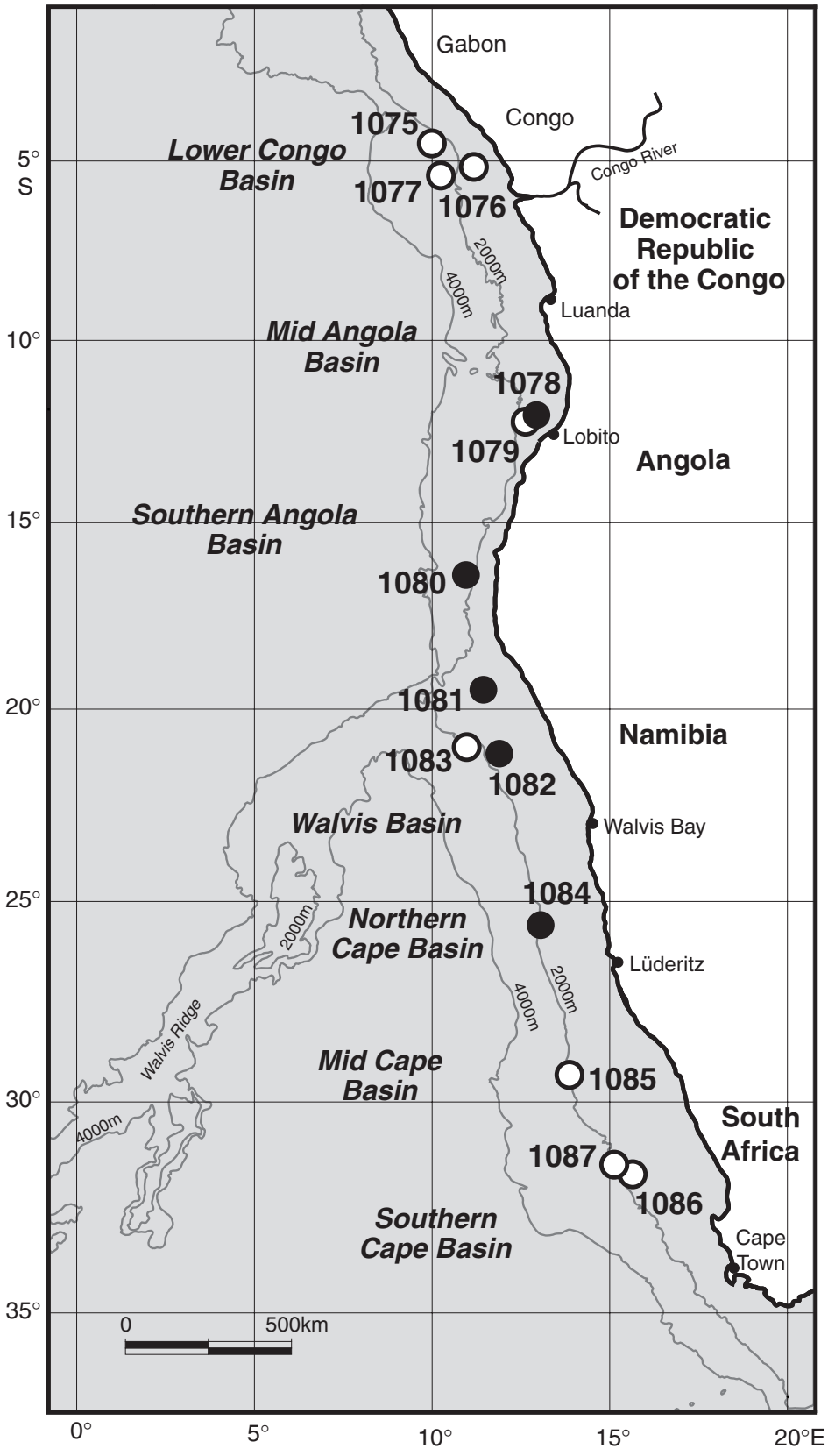

Figure F2. A. SEM-BSE photomicrograph showing the texture of a semilithified horizon. Note the high intercrystalline porosity (black) in relation to the lithified horizon and the small microcrystalline dolomicrite aggregates) in semilithified horizons. Horizon growth occurs through the coalescence of aggregates. The silt-sized subangular grains are detrital quartz clasts (q). **B.** SEM-BSE photomicrograph showing the texture of a diatom-rich lithified horizon. The elongate black areas are siliceous spicules (s). The round black areas and partially occluded round black areas are diatom tests (d). Note that pore spaces are almost completely occluded by dolomicrite (light gray color). **C.** CL photomicrograph of authigenically cemented Bouma DE turbidites from the Angola Basin. Turbidites are normally graded and have silt-sized detrital grains within their bases. Zoned dolomite grains (zd) have cores of detrital dolomite (luminescent) or authigenic pyrite crystals (black) and possess secondary luminescent dolomite rims. **D.** CL photomicrograph of slightly recrystallized foraminifer tests in a matrix of luminescent dolomicirite (dm). The arrow points to the outer margin of the shell wall where recrystallization has produced a thin luminescent intraparticle lining. **E.** Plane-light photomicrograph showing organic-rich blebs (o) and abundant pyrite grains (p) within a matrix of dolomicrite (dm). This texture is characteristic of dolomite samples examined in this study. **F.** SEM-BSE photomicrograph showing a foraminifer test partially occluded by blocky dolomite (bd) in a dolomicrite matrix (dm). **G.** Plane-light photomicrograph showing a diatom test partially occluded by blocky dolomite (bd) in a dolomicrite matrix (dm). **H.** CL photomicrograph of (G) showing the nonluminescent character of blocky dolomite and the mottled CL texture of the dolomicrite matrix. The bright specks are silt-sized grains of quartz that luminesce pale blue. (**Figure shown on next page.**)

Figure F2 (continued). (Caption shown on previous page.)

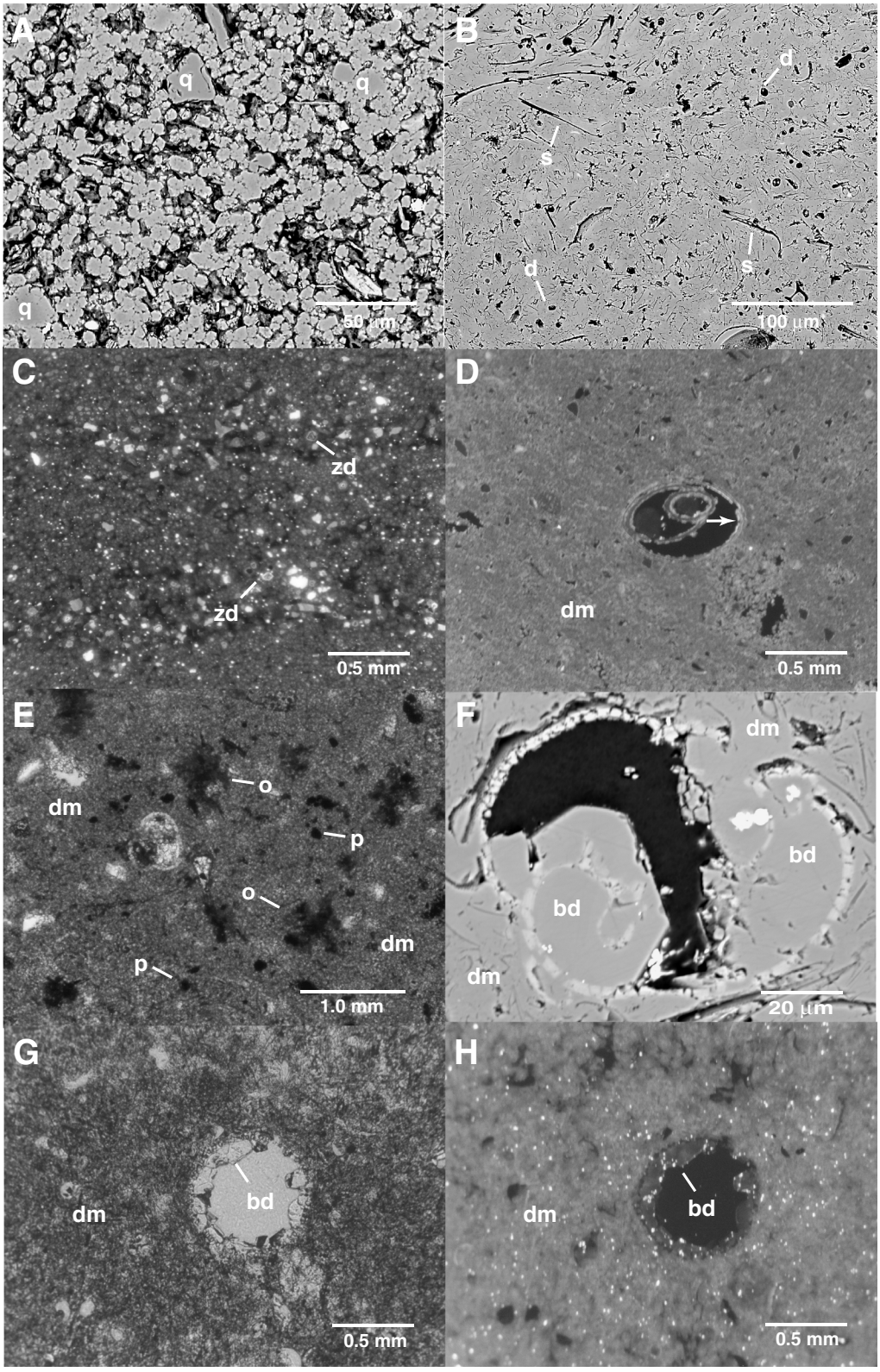

Figure F3. CL spectrum showing Mn-activated luminescence. The emission of Mn^{2+} in dolomite depends on the substitution site and is characterized by a main emission band between 590 and 620 nm and a strong secondary band between 640 and 680 nm (Machel et al., 1991). The first band is the result of Mn^{2+} substituting for Ca^{2+}, and the second records Mn^{2+} substituting for Mg^{2+}.

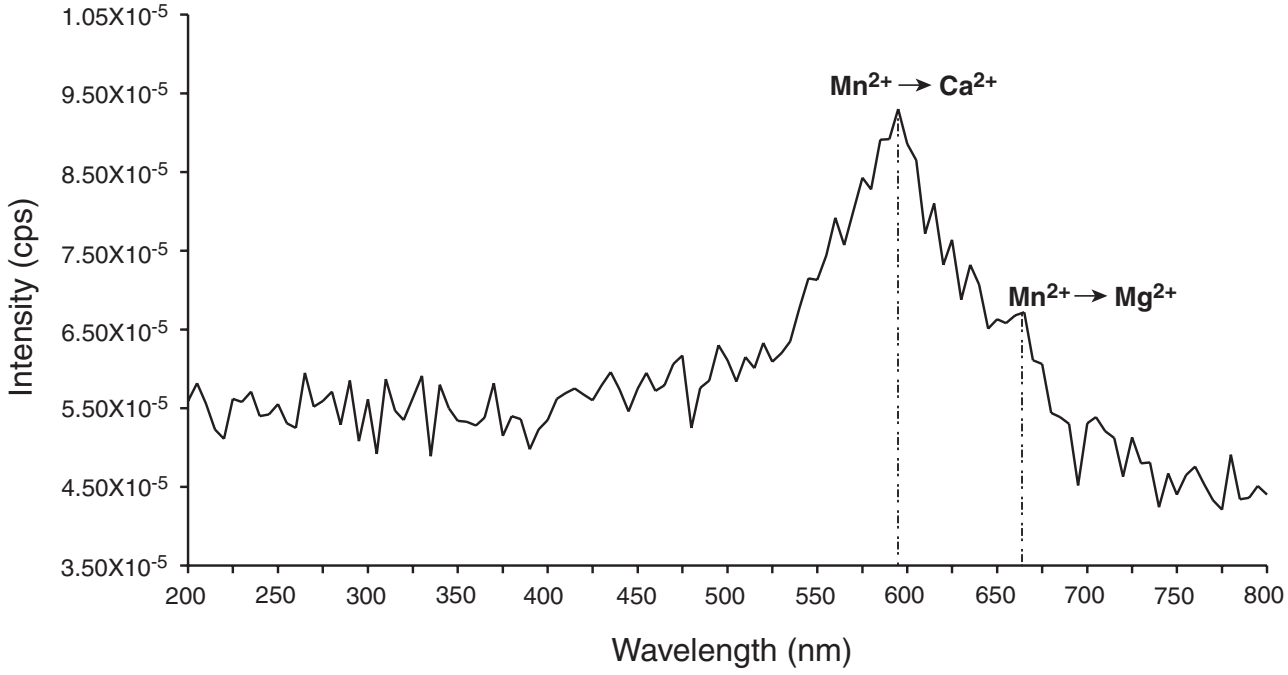

Figure F4. Typical X-ray diffractograms of semilithified and lithified horizons. Reflections are indexed based on the hexagonal reference system. Superstructure reflections (101), (015), (021), and (009) indicate that both semilithified and lithified horizons are formed of well-ordered dolomite. D = dolomite, Q = quartz, H = halite.

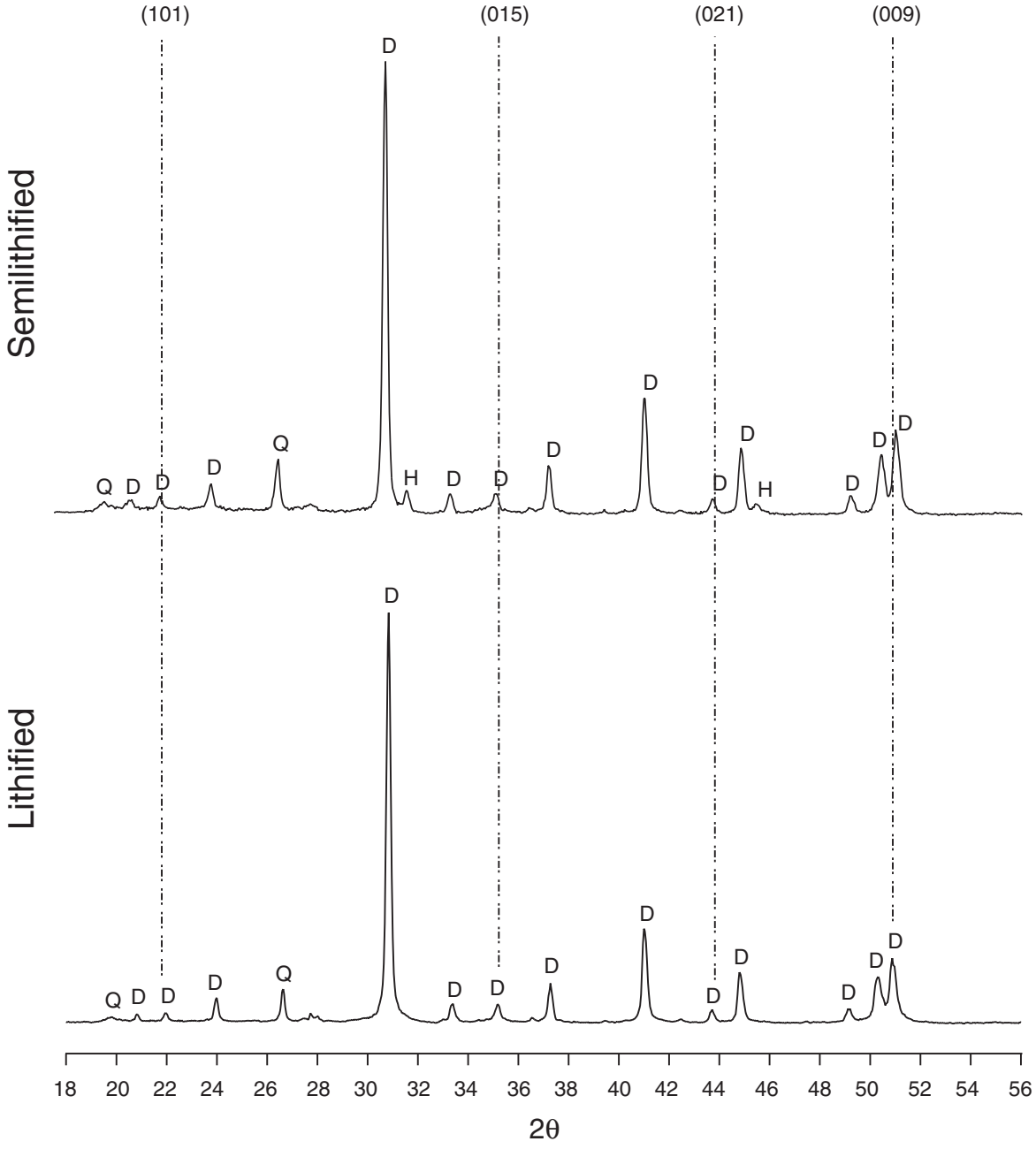

Table T1. Stratigraphic, compositional, luminescent, and isotopic data for dolomite samples.

Core, section, interval (cm)	Water depth (m)	Present depth of horizon (mbsf)	Lithology of host sediment	Age of host sediment	Productivity	TOC (wt%)	Sedimentation rate (cm/k.y.)	Horizon type	CL	$\delta^{13}C$ (‰ PDB)	$\delta^{18}O$ (‰ PDB)
175-1078C-											
13H-1, 43-46	427	111.63	nrsc	middle to late Pleistocene	Low	~2.3	~60	Lithified	WL	9.37	5.74
15X-2, 109-113	427	131.39	nrsc	middle to late Pleistocene	Low	~3.3	~60	Lithified	WL	8.64	5.78
175-1080A-											
7X-1, 5-12	2766	50.85	drsc	early to middle Pleistocene	Moderate	~2.4	~10	Lithified	WL	14.26	5.50
175-1081A-											
17X-1, 5-12	791	137.05	drc	late Pliocene	High	~8.2	~15	Semilithified	L	–3.63	5.71
19X-1, 0-6	791	155.00	drc	late Pliocene	High	~5.3	~9	Semilithified	L	3.81	6.19
20X-2, 62-67	791	166.50	drc	late Pliocene	High	~4.3	~9	Semilithified	L	5.24	5.86
20X-2, 86-89	791	166.70	drc	late Pliocene	High	~4.3	~9	Semilithified	L	5.10	6.18
20X-2, 92-94	791	168.80	drc	late Pliocene	High	~3.8	~9	Semilithified	L	5.63	5.89
22X-3, 11-15	791	186.50	drc	late Pliocene	High	~4.0	~9	Semilithified	L	7.64	5.61
22X-3, 29-32	791	186.60	drc	late Pliocene	High	~4.0	~9	Semilithified	L	7.72	5.74
25X-4, 138-141	791	218.05	dbc	late Pliocene	High	~4.8	~9	Semilithified	WL	7.40	5.71
175-1082A-											
15X-1, 0-8	1279	199.96	nrc	late Pliocene	High	~2.9	~21	Lithified	NL	12.87	6.19
22X-3, 114-125	1279	200.20	nrc	late Pliocene	High	~2.9	~21	Lithified	NL	13.25	5.44
36X-1, 5-14	1279	327.55	nrc	late Pliocene	High	~2.4	~10	Lithified	NL	11.72	4.19
175-1084A-											
18X-1, 0-4	1992	148.35	nrc	Pleistocene	Moderate	~3.5	~25	Lithified	NL	14.50	6.00
18X-1, 4-8	1992	148.45	nrc	Pleistocene	Moderate	~3.5	~25	Lithified	NL	16.85	6.50
18X-1, 8-15	1992	149.58	nrc	Pleistocene	Moderate	~3.5	~25	Lithified	NL	16.44	5.85
48X-1, 28-40	1992	468.55	do	Pleistocene	Moderate	~3.8	~10	Lithified	L	12.17	2.87

Notes: TOC = total organic carbon, CL = cathodoluminescence, PDB = peedee belemnite standard. Lithology: nrsc = nannofossil-rich silty clay, drsc = diatom-rich silty clay, drc = diatom-rich clay, dbc = diatom-bearing clay, nrc = nannofossil-rich clay, do = diatom ooze. CL rating: WL = weakly luminescent dolomicrite, L = luminescent dolomicrite, NL = nonluminescent dolomicrite. TOC of host sediment at specified depth interval is estimated from onboard calculations.

Table T2. Electron microprobe analyses of iron concentrations within weakly luminescent dolomicrite, luminescent dolomicrite, and blocky dolomite from various Leg 175 dolomites.

Weakly luminescent dolomicrite		Luminescent dolomite		Blocky dolomite	
Core, section, interval (cm)	Fe (APFU)	Core, section, interval (cm)	Fe (APFU)	Core, section, interval (cm)	Fe (APFU)
175-1082A-		175-1081A-		175-1082A-	
15X-1, 0-8	0.019	17X-1, 5-12	0.009	22X-3, 114-125	0.021
15X-1, 0-8	0.028	17X-1, 5-12	0.000	22X-3, 114-125	0.021
15X-1, 0-8	0.017	17X-1, 5-12	0.001	22X-3, 114-125	0.013
15X-1, 0-8	0.028	17X-1, 5-12	0.001	22X-3, 114-125	0.022
15X-1, 0-8	0.005	17X-1, 5-12	0.009	22X-3, 114-125	0.019
15X-1, 0-8	0.026	17X-1, 5-12	0.001	22X-3, 114-125	0.026
15X-1, 0-8	0.019			22X-3, 114-125	0.034
22X-3, 114-125	0.012	175-1084A-		22X-3, 114-125	0.017
22X-3, 114-125	0.002	48X-1, 28-40	0.013	22X-3, 114-125	0.003
22X-3, 114-125	0.029	48X-1, 28-40	0.002	22X-3, 114-125	0.006
22X-3, 114-125	0.014	48X-1, 28-40	0.015	22X-3, 114-125	0.006
22X-3, 114-125	0.017	48X-1, 28-40	0.001		
22X-3, 114-125	0.005	48X-1, 28-40	0.017	175-1084A-	
22X-3, 114-125	0.023	48X-1, 28-40	0.013	48X-1, 28-40	0.023
22X-3, 114-125	0.015	48X-1, 28-40	0.001	48X-1, 28-40	0.035
22X-3, 114-125	0.011	48X-1, 28-40	0.001	48X-1, 28-40	0.025
22X-3, 114-125	0.004	48X-1, 28-40	0.006	48X-1, 28-40	0.015
22X-3, 114-125	0.006	48X-1, 28-40	0.002	48X-1, 28-40	0.042
22X-3, 114-125	0.025	48X-1, 28-40	0.001	48X-1, 28-40	0.026
22X-3, 114-125	0.002	48X-1, 28-40	0.001	48X-1, 28-40	0.023
22X-3, 114-125	0.032	48X-1, 28-40	0.001	48X-1, 28-40	0.028
		48X-1, 28-40	0.001	48X-1, 28-40	0.003
				48X-1, 28-40	0.029
				48X-1, 28-40	0.036
				48X-1, 28-40	0.027
				48X-1, 28-40	0.038
Average:	0.016 ± 0.010	Average:	0.005 ± 0.005	Average:	0.022 ± 0.011

Notes: APFU = atoms per formula unit. Electron microprobe analysis of zoned dolomite was not possible because of its small crystal size (<12 µm) and disseminated nature.